

Oveissi, Parham, et al. "Learning-based Adaptive Thrust Regulation of Solid Fuel Ramjet" AIAA SCITECH 2023 Forum 23-27 January 2023.  
<https://doi.org/10.2514/6.2023-2533>.

<https://doi.org/10.2514/6.2023-2533>

Access to this work was provided by the University of Maryland, Baltimore County (UMBC) ScholarWorks@UMBC digital repository on the Maryland Shared Open Access (MD-SOAR) platform.

**Please provide feedback**

Please support the ScholarWorks@UMBC repository by emailing [scholarworks-group@umbc.edu](mailto:scholarworks-group@umbc.edu) and telling us what having access to this work means to you and why it's important to you. Thank you.

# Learning-based, Adaptive Thrust Regulation of Solid Fuel Ramjet

Parham Oveissi\*, Arjun Trivedi†, Ankit Goel‡,  
*Department of Mechanical Engineering, University of Maryland, Baltimore County*

Ozgur Tumuklu§, Kyle Hanquist¶,  
*Department of Aerospace and Mechanical Engineering, University of Arizona*

Douglas Philbrick||, Alireza Farahmandi\*\*,  
*Naval Air Warfare Center, China Lake, California*

**This paper uses retrospective cost adaptive control to regulate the thrust generated by a solid fuel ramjet engine. A one-dimensional quasi-static model based on the conservation of mass, momentum, and energy, along with a simplified regression model for solid fuel combustion, is used to model the solid fuel ramjet engine. We use the SFRJ model in open-loop simulations to establish the operational envelope of the engine. Then, RCAC is tuned to regulate the thrust produced by the engine in nominal and off-nominal operating conditions. The performance of the adaptive controller is compared with a fixed-gain controller optimized by RCAC under nominal operating conditions. In each case, it is observed that the RCAC significantly improves the transient performance.**

## Nomenclature

$A_i$	=	cross-sectional area at station $i$
$P$	=	pressure
$T$	=	temperature
$\dot{m}$	=	mass-flow rate
$\phi$	=	equivalence ratio
$r_k$	=	command at step $k$
$y_k$	=	measured output at step $k$
$z_k$	=	error signal at step $k$
$u_k$	=	controller output at step $k$
$\theta_k$	=	controller coefficients at step $k$

## I. Introduction

A key technological challenge in developing cost-effective hypersonic vehicles is a reliable propulsion system. Since hypersonic vehicles operate at very high speeds, the propulsion system must be lightweight and have a high thrust output. A ramjet engine, due to its simple design and operation, satisfies both of these requirements. A ramjet engine uses the forward motion of the engine to compress the incoming air. The inlet duct is designed in such a way that in the operating range, the incoming flow passes through a carefully designed supersonic shock structure, resulting in a high-pressure and high-temperature flow in the combustor. Under these conditions, the fuel in the combustion chamber spontaneously

---

\*Graduate Student, Department of Mechanical Engineering, 1000 Hilltop Circle, Baltimore, MD 21250.

†Undergraduate Student, Department of Mechanical Engineering, 1000 Hilltop Circle, Baltimore, MD 21250.

‡Assistant Professor, Department of Mechanical Engineering, 1000 Hilltop Circle, Baltimore, MD 21250.

§Postdoctoral Research Associate, Aerospace and Mechanical Engineering Department, Tucson, AZ 85721, AIAA Member.

¶Assistant Professor, Department of Aerospace & Mechanical Engineering, 1130 N. Mountain Avenue, University of Arizona, Tucson, AZ 85721, AIAA Senior Member.

||Senior Researcher, Naval Air Warfare Center Weapons Division, China Lake, CA 93555.

\*\*Researcher, Naval Air Warfare Center Weapons Division, China Lake, CA 93555.

ignites and adds energy to the flow. The high-energy flow then exhausts through the nozzle, thereby generating forward thrust. Ramjet engines can reliably produce steady, extended-duration thrust, and thus are particularly well-suited for long-range operation at high speeds. The lack of rotating turbomachinery makes the ramjet much simpler than other types of air-breathing propulsion systems. Ramjets can be further classified as liquid-fuel (LFRJ) or solid-fuel (SFRJ) ramjets. Since an SFRJ does not require turbopumps, fuel bladders, injectors and associated plumbing, it is much simpler than a comparably-sized LFRJ, and has the added advantage that it can be stored as a “wooden round”, without the logistical concerns associated with liquid fuels. Due to the higher volumetric energy density of solid fuel, the SFRJ has the potential for a greater range than the LFRJ. Additionally, since the combustion flame front spans the entire length of the fuel grain, SFRJs are less likely than LFRJs to suffer from combustion instabilities.

A typical SFRJ geometry is shown in Figure 1. The lining of the combustor is the solid fuel grain. The high-speed, high-temperature flow vaporizes and ignites the fuel, thus adding energy to the flow, and resulting in the generation of thrust. If the airflow rate is too low, heat addition might be insufficient to generate the necessary thrust, whereas if the flow rate is too high, the inlet may unstart due to excessive heat addition, or the combustion blowoff limits may be exceeded. Each of these scenarios can lead to flame extinction and loss of thrust. Therefore, the thermodynamic state (the pressure, temperature, and the flow rate at the combustor) must be maintained within a fairly narrow range of operating conditions. Because of the complexity of the multi-physics processes involved (solid combustion, mixing, and high-speed flow), this range can be extremely difficult to predict analytically. Reliable operation of SFRJ thus requires an approach to maintaining the state of the SFRJ within acceptable limits over as wide an operating envelope as possible. To date, the approach to achieve this consists of passive, open-loop control strategies, implemented by careful geometric design of the combustor and fuel grain.

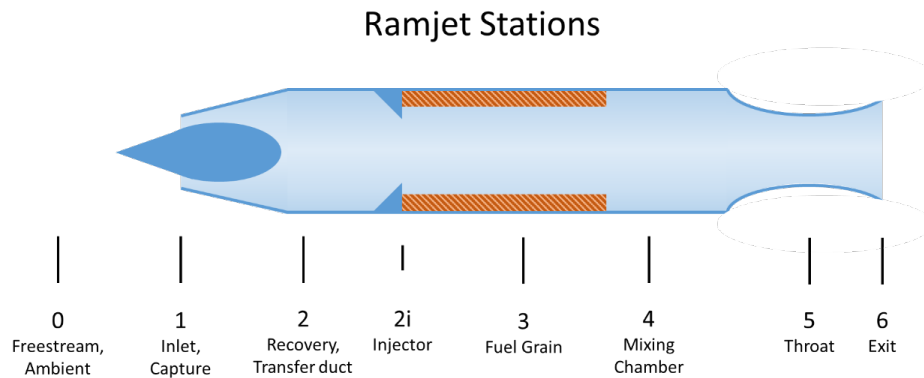


Fig. 1 A typical SFRJ cross-section with various stations.

Thrust modulation of SFRJ has been an active area of research for over four decades. Since the 1980s, several researchers have developed computational code to simulate the flow conditions inside an SFRJ [1–5]. These numerical simulations highlighted the complex flow interaction and qualitatively showed the response of an SFRJ in steady-state conditions.

In order to regulate the thrust generated by an SFRJ, several researchers developed and validated algebraic relations between the flow rate and the thrust generated by an SFRJ in static conditions using conservation of mass, momentum, and energy equations and quasi-static flow assumptions [2, 5–9]. The effect of disturbances on the flow was considered in [10]. Importantly, these approaches rely on accurate knowledge of the physical parameters of the SFRJ. Measurement inaccuracies propagate to incorrect input computation, and thus to incorrect thrust output. Furthermore, these *static* (open loop?) control laws were validated only in benign flow conditions. In order to compensate for uncertainty and unmodeled physics, closed-loop control techniques to regulate the thrust generated by SFRJ were explored in [11, 12]. In [11], the simplified ODE was used to develop an adaptive controller to regulate the thrust. However, the adaptive controller was validated only in simulation. Furthermore, the resulting control system was only demonstrated to regulate the output of the system as modeled by ODEs, not by the more realistic and physically motivated PDEs.

In our recent work described in [13–15], we developed an adaptive control system to regulate the thrust and prevent inlet unstart in a liquid-fuel scramjet engine. The adaptive control system was based on retrospective cost optimization, where an auxiliary cost function, based on measured data and past inputs, is optimized to continually update the control law. This control technique, known as retrospective cost adaptive control (RCAC) requires minimal modeling information. In most applications, a simple first-order transfer function, which can be easily obtained by open-loop

simulation of the system, or from experimentally collected data, is sufficient.

A key feature of RCAC that makes it particularly attractive to flow-control problems is its ability to adapt online as necessary. Furthermore, since RCAC requires only measured data (and not a system model) to optimize the controller, it can be directly integrated with a numerical simulation for purposes of training and stress testing. These features enable RCAC to be tuned using a computationally simple simulation of the system, and to then adapt in an appropriate way to a more realistic simulation, or to the physical system itself.

In this paper, we investigate the application of RCAC to regulate the thrust generated by an SFRJ using only measured output data. A one-dimensional quasi-static model based on the conservation of mass, momentum, and energy and a simplified regression model for energy release is used to model the SFRJ. In order to use a discrete-time closed-loop control to regulate the thrust, we assume that the dynamics of the SFRJ are faster than the control signal updates, that is, the SFRJ states converge between the samples. This crucial assumption allows us to use a static model in a basic servo loop to construct a dynamic controller for SFRJ thrust regulation.

The main contribution of this work is the demonstration of model-free, learning-based, adaptive regulation of the SFRJ thrust with unknown and uncertain dynamics. The paper is organized as follows. Section II describes the one-dimensional static model of the SFRJ, Section III briefly reviews the RCAC algorithm, and Section IV presents simulation results. Finally, the paper concludes in section V.

## II. Solid Fuel Ramjet Model

In this work, we consider a static model of the SFRJ, that is, for a given value of the bypass ratio (BPR), the model computes the steady state value of the generated thrust. The use of bypass air as a means to affect the SFRJ thrust is described in [16]. The static model consists of a set of implicit algebraic equations that are solved to compute the steady-state thrust for a given BPR. In particular, the model assumes steady inlet conditions, equilibrium composition during the expansion, and frozen chemical compositions at the combustion chamber to compute the Mach numbers at the stations shown in Figure 1.

We assume that the geometric configuration of the engine, that is, the inlet area  $A_1$  to the exit area  $A_6$ , is known. Using isentropic flow conditions along with freestream pressure  $P_0$  and temperature  $T_0$  at the operational altitude the inlet air mass flow rate is given by

$$\dot{m}_0 = M_0 P_0 A_0 \sqrt{\frac{\gamma_0 w_0}{R_u T_0}}, \quad (1)$$

where  $R_u$  is the universal gas constant,  $\gamma_0$  is the freestream specific heat ratio, and  $M_0$ ,  $T_0$ ,  $P_0$ , and  $w_0$  are the freestream Mach number, temperature, and pressure, and the molar mass for air, respectively. The proportion of  $\dot{m}_0$  that passes through the center of the fuel grain depends on the BPR  $\beta$ , and is given by

$$\dot{m}_3 = \dot{m}_0(1 - \beta). \quad (2)$$

Since the governing equations form an implicit nonlinear algebraic system, an iterative method is used to compute the solution. In particular, the equations are iteratively solved with an initial guess of the static pressure in the mixing chamber  $P_4$ ,  $M_4$ , and  $\gamma_4$ , until  $P_4$  converges, as described below. Using the current estimate of  $P_4$ , the fuel grain regression rate is computed by

$$\dot{r} = \alpha \left( \frac{\dot{m}_3}{A_3} \right)^a P_4^b T_{t2}^c, \quad (3)$$

where  $T_{t2}$  is the total temperature at station 2, assumed to be equal to the freestream total temperature, and  $\alpha$ ,  $a$ ,  $b$ , and  $c$  are experimentally-determined constants specific to the motor geometry and the fuel type, assumed to be HTPB in this study. Note that (3) is an empirical relation that has been determined experimentally. Finally, the fuel consumption rate is computed as

$$\dot{m}_f = \rho_f A_f \dot{r} \quad (4)$$

where  $A_f$  is the exposed surface area of the fuel grain and  $\rho_f$  is the fuel density. Next, defining the equivalence ratio as

$$\phi \triangleq \frac{(\dot{m}_f / \dot{m}_0)}{(F/A)_s}, \quad (5)$$

where  $(F/A)_s$  is the stoichiometric fuel-air ratio for HTPB, and computing the total pressure at station 4 using the isentropic relationship

$$P_{t4} = P_4 \left( 1 + \frac{\gamma_4 - 1}{2} M_4^2 \right)^{\frac{\gamma_4}{\gamma_4 - 1}}, \quad (6)$$

NASA's CEA code [17] is used to compute post-combustion gas properties downstream of the mixing chamber using  $\phi$ ,  $T_{t2}$ , and  $P_{t4}$ , as inputs. In our application, the relevant outputs are  $T_{t4}$ ,  $\gamma_4$ , and  $w_4$ . A traditional approach, based on long experience with data collected from laboratory experiments, is to use the value for  $\gamma_4$  computed by CEA as the value of  $\gamma$  at stations 4, 5, and 6 in all subsequent calculations, and we will refer to this value simply as  $\gamma$ . In practice, any inconsistencies introduced by this assumption are accounted for by using a calibrated value for combustion efficiency. The Mach number at station 4 is then computed by solving the isentropic area-ratio relation

$$\frac{A_4}{A_5} = \frac{1}{M_4} \left( \frac{2 + (\gamma - 1)M_4^2}{\gamma + 1} \right)^{\frac{\gamma + 1}{2(\gamma - 1)}} \quad (7)$$

where the subsonic solution for  $M_4$  is used. The total pressure at station 5 is calculated using the sonic conditions at the nozzle throat (see equation 3.119 in [18])

$$P_{t5} = \frac{\dot{m}_5 \sqrt{\frac{R_u T_{t4}}{w_4}}}{C A_5 \left[ \gamma^{0.5} \left( \frac{2}{\gamma + 1} \right)^{\frac{\gamma + 1}{2(\gamma - 1)}} \right]} \quad (8)$$

where  $C$  is the nozzle discharge coefficient and  $\dot{m}_5 = \dot{m}_0 + \dot{m}_f$ . Next, using the assumption that  $P_{t4} = P_{t5} = P_{t6}$ , we calculate an updated value of  $P_4$ .

$$P_{4\text{New}} = \frac{P_{t5}}{\left( 1 + \frac{\gamma - 1}{2} M_4^2 \right)^{\frac{\gamma}{\gamma - 1}}}, \quad (9)$$

At this point, we compare the previous value of  $P_4$  with  $P_{4\text{New}}$ . When the difference between the two is below a threshold value,  $P_4$  is assumed to have converged. Otherwise,  $P_4$  is set equal to the average of the two values and the equations (3)-(9) is repeated. In practice, this algorithm converges within a few iterations using a reasonable threshold value.

Finally,  $M_6$  is computed by solving

$$\frac{A_6}{A_5} = \frac{1}{M_6} \left( \frac{2 + (\gamma - 1)M_6^2}{\gamma + 1} \right)^{\frac{\gamma + 1}{2(\gamma - 1)}} \quad (10)$$

and choosing the supersonic solution for  $M_6$ . Then the exit pressure,  $P_6$ , is calculated using

$$P_6 = \frac{P_{t5}}{\left( 1 + \frac{\gamma - 1}{2} M_6^2 \right)^{\frac{\gamma}{\gamma - 1}}}, \quad (11)$$

Finally, the net thrust  $F_{\text{net}}$  is given by

$$F_{\text{net}} = \varphi \left( P_6 A_6 \gamma M_6^2 + P_6 A_6 \right) - A_6 P_0 - P_0 A_0 \gamma_0 M_0^2 \quad (12)$$

where  $\varphi$  is a thrust efficiency parameter and is assumed to be unity in this work. Furthermore, in this work, the various station areas are  $A_0 = 0.020325 \text{ m}^2$ ,  $A_4 = 0.022698 \text{ m}^2$ ,  $A_5 = 0.032 \text{ m}^2$ , and  $A_6 = 0.048 \text{ m}^2$ .

### III. RCAC Algorithm

This section briefly reviews the retrospective cost adaptive control (RCAC) algorithm. RCAC is described in detail in [19] and its extension to digital PID control is given in [20]. Consider a system

$$x_{k+1} = f(k, x_k, u_k, w_k), \quad (13)$$

$$y_k = g(k, x_k, w_k), \quad (14)$$

where  $x_k \in \mathbb{R}^{l_x}$  is the state,  $u_k \in \mathbb{R}^{l_u}$  is the input,  $y_k \in \mathbb{R}^{l_y}$  is the measured output, and  $w_k \in \mathbb{R}^{l_w}$  is the exogenous signal that can represent commands, external disturbance, or both. The functions  $f$  and  $g$  represent the dynamics map and the output map. The goal is to develop an adaptive control law that drives the output  $y_k$  to desired values with limited modeling information about (13), (14). Note that explicit knowledge of  $f$  and  $g$  is not required since RCAC requires only the input and output measurements.

Consider a linearly parameterized control law

$$u_k = \Phi_k \theta_k, \quad (15)$$

where  $\Phi_k \in \mathbb{R}^{l_u \times l_\theta}$  is the regressor matrix that is constructed using the measured data and  $\theta_k \in \mathbb{R}^{l_\theta}$  is the vector of the controller coefficients optimized by RCAC at step  $k$ . For example, a discrete-time PID control law can be written in the regressor form given by (15), where, at step  $k$ ,

$$\Phi_k \triangleq \begin{bmatrix} z_k & \gamma_k & z_k - z_{k-1} \end{bmatrix}, \theta_k = \begin{bmatrix} K_{p,k} \\ K_{i,k} \\ K_{d,k} \end{bmatrix}, \quad (16)$$

$\gamma_k = \sum_i z_i$  is the accumulated error, and  $K_{p,k}$ ,  $K_{i,k}$ , and  $K_{d,k}$  are the proportional, integral, and derivative gains, respectively. Various MIMO controller parameterizations of the control law (15) are shown in [21]. To determine the controller gains  $\theta_k$ , let  $\theta \in \mathbb{R}^{l_\theta}$ , and consider the *retrospective performance variable* defined by

$$\hat{z}_k(\theta) \triangleq g(z_k) + G_f(\mathbf{q})(\Phi_k \theta - u_k), \quad (17)$$

where

$$G_f(\mathbf{q}) \triangleq \sum_{i=1}^{n_f} \frac{N_i}{\mathbf{q}^i} \quad (18)$$

is an FIR filter. Note that  $N_i \in \mathbb{R}^{l_z \times l_u}$ . Furthermore, define the *retrospective cost function*  $J_k: \mathbb{R}^{l_\theta} \rightarrow [0, \infty)$  by

$$J_k(\theta) \triangleq \sum_{i=0}^k \hat{z}_i(\theta)^T R_z \hat{z}_i(\theta) + (\Phi_k \theta)^T R_u (\Phi_k \theta) + (\theta - \theta_0)^T P_0^{-1} (\theta - \theta_0), \quad (19)$$

where  $R_z \in \mathbb{R}^{l_z \times l_z}$ ,  $R_u \in \mathbb{R}^{l_u \times l_u}$ , and  $P_0 \in \mathbb{R}^{l_\theta \times l_\theta}$  are positive definite; and  $\theta_0 \in \mathbb{R}^{l_\theta}$  is the initial vector of controller gains.

**Proposition III.1** Consider (19), where  $\theta_0 \in \mathbb{R}^{l_\theta}$  and  $P_0 \in \mathbb{R}^{l_\theta \times l_\theta}$  is positive definite. For all  $k \geq 0$ , denote the minimizer of  $J_k$  given by (19) by

$$\theta_{k+1} \triangleq \underset{\theta \in \mathbb{R}^n}{\operatorname{argmin}} J_k(\theta). \quad (20)$$

Then, for all  $k \geq 0$ ,  $\theta_{k+1}$  is given by

$$\theta_{k+1} = \theta_k - P_{k+1} \Phi_{f,k}^T R_z (z_k + \Phi_{f,k} \theta_k - u_{f,k}) - P_{k+1} \Phi_k^T R_u \Phi_k \theta_k, \quad (21)$$

where

$$P_{k+1} = P_k - P_k \bar{\Phi}_k^T \left( \bar{R}^{-1} + \bar{\Phi}_k P_k \bar{\Phi}_k^T \right)^{-1} \bar{\Phi}_k P_k, \quad (22)$$

and

$$\Phi_{f,k} \triangleq G_f(\mathbf{q}) \Phi_k, \quad u_{f,k} \triangleq G_f(\mathbf{q}) u_k, \quad \bar{\Phi}_k \triangleq \begin{bmatrix} \Phi_{f,k} \\ \Phi_k \end{bmatrix}, \quad \bar{R} \triangleq \begin{bmatrix} R_z & 0 \\ 0 & R_u \end{bmatrix}. \quad (23)$$

**Proof:** See [22]

Finally, the control is given by

$$u_{k+1} = \Phi_{k+1} \theta_{k+1}. \quad (24)$$

#### IV. Simulation Results

In this section, we investigate the performance of the learning controller to regulate the thrust generated by the SFRJ in presence of parametric uncertainties. The control system architecture to regulate the SFRJ thrust is shown in Figure 2. At step  $k$ , the commanded thrust is denoted by  $r_k$ , the thrust generated by the SFRJ is denoted by  $y_k$ , and the BPR  $\beta_k = \beta_0 + u_k$ , where  $\beta_0 = 0.5$  and  $u_k$  is the controller output computed by the RCAC algorithm. The error signal  $z_k \triangleq r_k - y_k$  is used both to update the RCAC control law and to drive the adaptive controller.

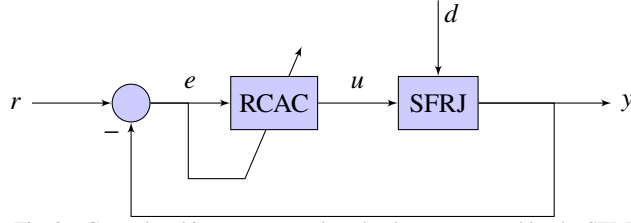


Fig. 2 Control architecture to regulate the thrust generated by the SFRJ.

In order to establish feasible thrust commands, we compute the thrust generated by the SFRJ for various bypass ratios at constant inlet conditions. The nominal operating conditions are assumed to be  $M_0 = 2$ ,  $T_0 = 480$  K, and  $P_0 = 10$  atm. Figure 3 shows the open-loop responses of the SFRJ at several operating conditions. In particular, the subplots show the SFRJ thrust as the inlet Mach number is increased from 1 to 3, the inlet total temperature is increased from 280 K to 680 K, the inlet total pressure is increased from 6 atm to 14 atm, and the combustion efficiency is increased from 75% to 95%, respectively. Note that in each case, the rest of the operating conditions are assumed to be the same as the nominal operating conditions. The open-loop responses show the range of thrust that can be generated by the SFRJ at a given operating condition. The higher values of BPR imply that less air is routed through the engine, and thus the generated thrust is lower, however, in practice, this range may be unknown. Nonetheless, for the purpose of investigating the effectiveness of the adaptive controller, we assume that the thrust commands are feasible; that is, there exists a value of the bypass ratio that will yield the desired thrust. Finally, Figure 4 shows the maximum thrust that can be generated by the SFRJ as a function of operating conditions.

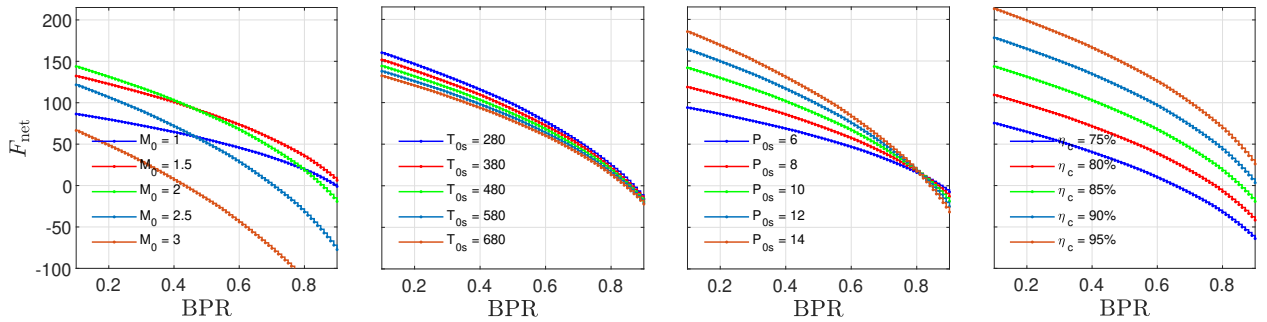


Fig. 3 Open-loop steady-state thrust output of the SFRJ obtained with constant values of the bypass ratio at various operating conditions.

Next, we use RCAC to regulate the thrust produced by the SFRJ under nominal operating conditions, which are assumed to be  $M_0 = 2$ ,  $T_0 = 480$ , and  $P_0 = 10$ . At these operating conditions, feasible reference commands are chosen using the open-loop response shown in Figure 3. Furthermore, reference commands are changed after every 500 steps. In RCAC, we set  $P_0 = 10^{-10}I_3$ ,  $R_u = 0$ ,  $N_1 = 10$ , and  $\theta_0 = 0$ . Figure 5 shows the closed-loop response, the first subplot shows the commanded and the generated thrust, the second subplot shows the control signal updated by RCAC, the third subplot shows the absolute value of the error signal on a log scale, and the fourth subplot shows the controller gains updated by RCAC at each step. Note that RCAC updates the control law (15) using only the error signal  $z_k$  and the past control signal  $u_k$ .

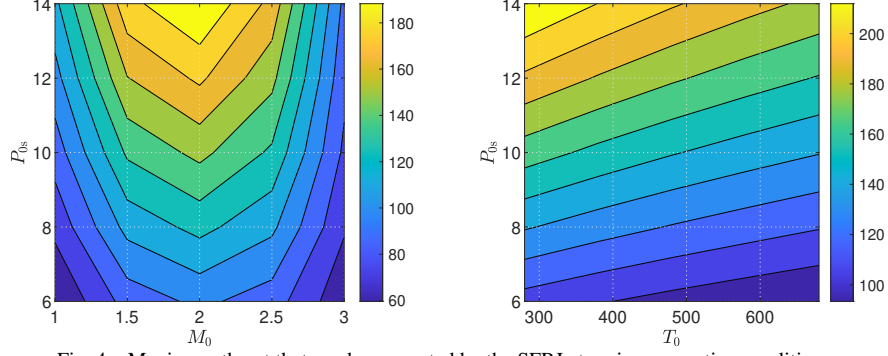


Fig. 4 Maximum thrust that can be generated by the SFRJ at various operating conditions.

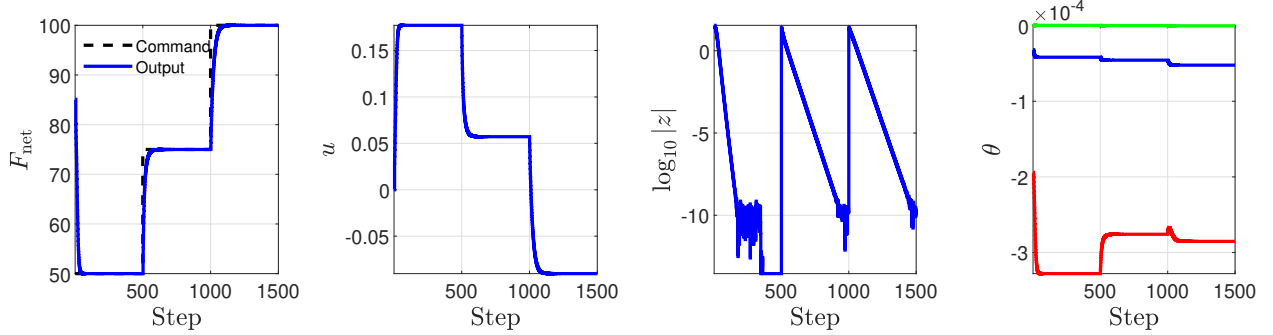


Fig. 5 Closed-loop response of the SFRJ to a sequence of step commands.

Next, we investigate the performance of the adaptive controller under uncertainties in the SFRJ model and changes in the operating conditions. Specifically, we vary the inlet Mach number, the total inlet pressure, the total inlet temperature, and the combustion efficiency in the SFRJ model and investigate the closed-loop transient and steady-state response with the adaptive controller in the loop. Note that RCAC hyperparameters are not retuned in the numerical experiment where uncertain parameters are varied. Furthermore, to quantify the performance of the adaptive controller, we compare its performance with a fixed-gain controller, where the fixed gains are selected to be the gains optimized by RCAC in the nominal operating case, that is, the gains obtained at the end of the simulation in Figure 5.

First, we vary the operating conditions by varying the inlet Mach number. The first subplot in Figure 3 shows the effect of inlet Mach number on the SFRJ thrust. The SFRJ is commanded to follow a sequence of step thrust commands. Figure 6 shows the thrust output of the SFRJ in the first row, the performance variable on a logarithmic scale in the second row, and the control input in the third row. The inlet Mach number is shown on top of each column. Note that red traces correspond to the fixed-gain controller and the blue traces correspond to the adaptive controller. Although the fixed-gain controller in the closed loop ensures asymptotic tracking of the step commands, the adaptive controller yields significantly faster convergence to the command in every case.

Next, we vary the operating conditions by varying the total inlet pressure in the SFRJ model. The second subplot in Figure 3 shows the effect of the total inlet pressure on the SFRJ thrust. Similar to the previous case, the SFRJ is commanded to follow a sequence of step thrust commands. Figure 7 shows the thrust output of the SFRJ in the first row, the performance variable on a logarithmic scale in the second row, and the control input in the third row. The total inlet pressure is shown on top of each column. Note that red traces correspond to the fixed-gain controller and the blue traces correspond to the adaptive controller. Although the fixed-gain controller in the closed loop ensures asymptotic tracking of the step commands, the adaptive controller yields significantly faster convergence to the command in all cases where the total inlet pressure is varied in every case.

Similarly, Figures 8 and 9 show the thrust output of the SFRJ in the first row, the performance variable on a logarithmic scale in the second row, and the control input in the third row, in the case where the total inlet temperature and the combustion efficiency is varied, respectively. The total inlet temperature and the combustion efficiency are shown on top of each column in both figures, respectively. Similar to the previous cases, although the fixed-gain controller in the closed loop ensures asymptotic tracking of the step commands, the adaptive controller yields significantly faster convergence to the command in all cases where the total inlet pressure is varied in every case.



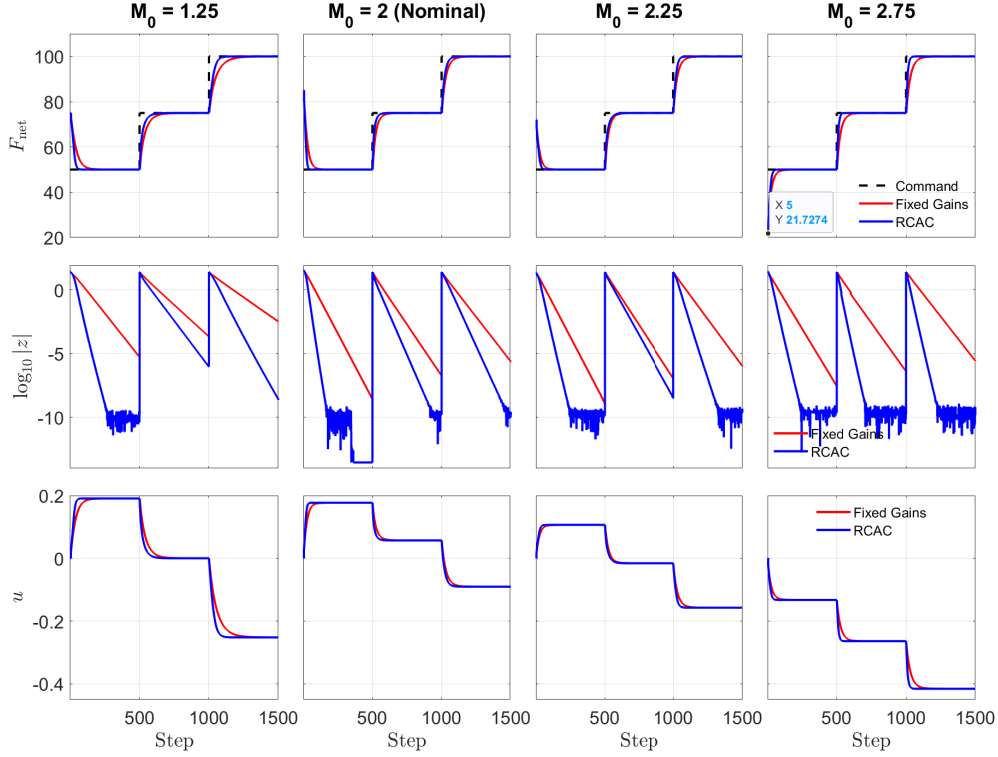


Fig. 6 Closed-loop response of the SFRJ with the fixed-gain PID and the RCAC PID controller as the inlet Mach number  $M_0$  is varied. The figures in the top row show the thrust generated by the SFRJ, the performance variable on a logarithmic scale is shown in the middle row, and the figures in the bottom row show the control signal. Note that RCAC adjusts the controller gains continually to improve the transient response.

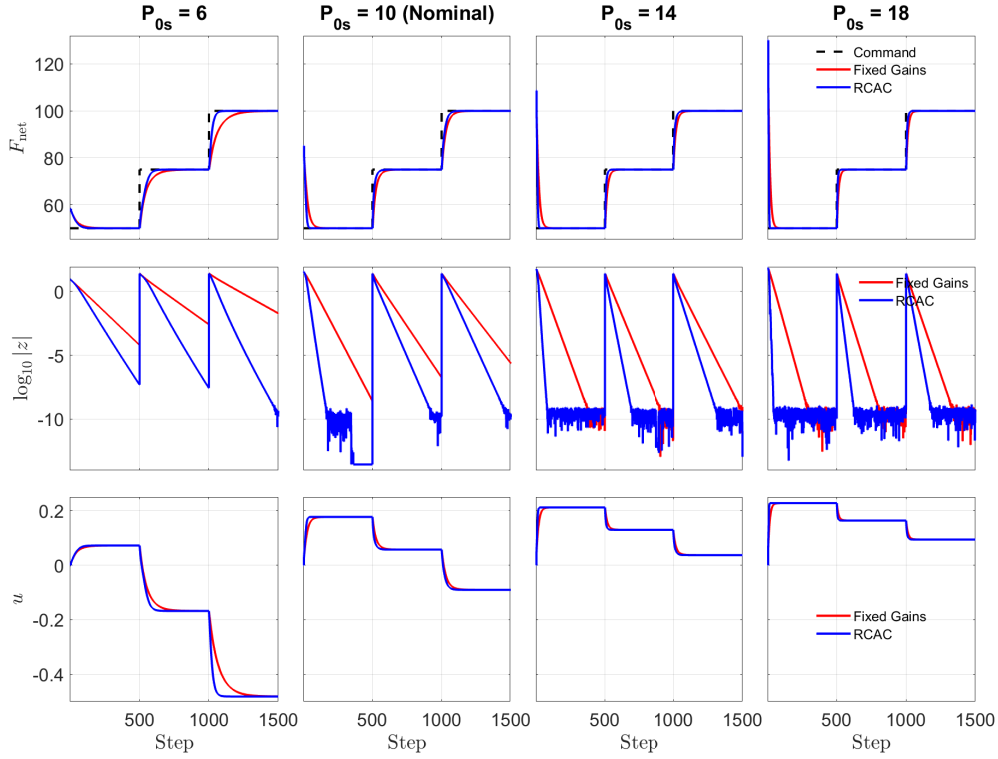


Fig. 7 Closed-loop response of the SFRJ with the fixed-gain PID and the RCAC PID controller as the inlet total pressure  $P_{0s}$  varies. The figures in the top row show the thrust generated by the SFRJ, the performance variable on a logarithmic scale is shown in the middle row, and the figures in the bottom row show the control signal. Note that RCAC adjusts the controller gains continually to improve the transient response.

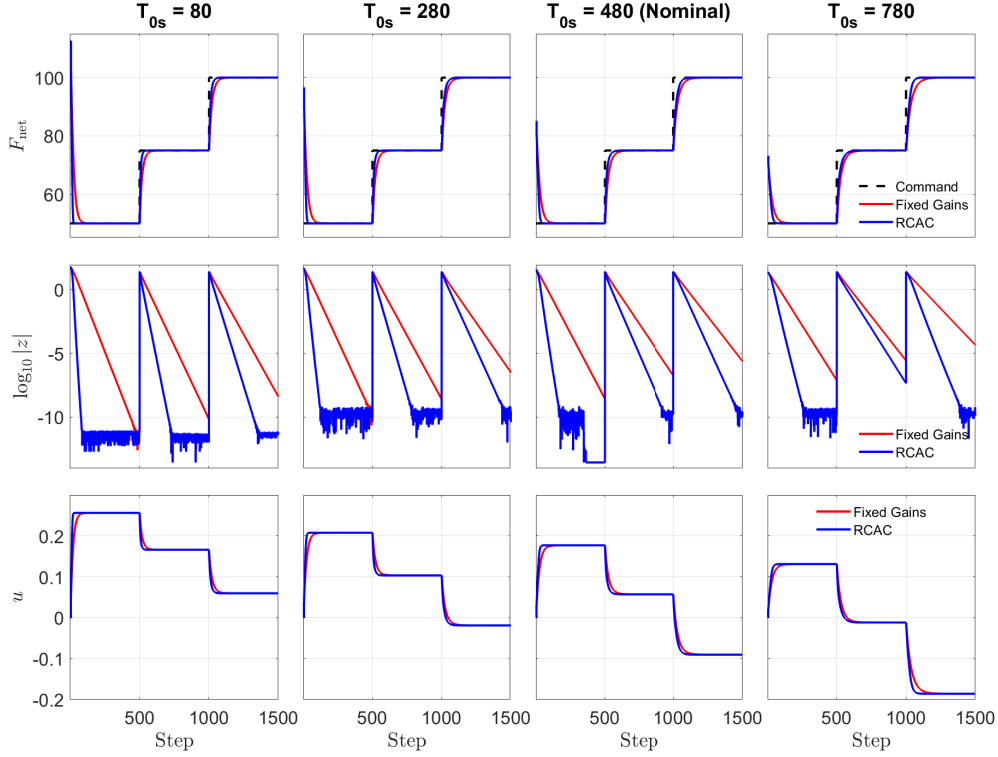


Fig. 8 Closed-loop response of the SFRJ with the fixed-gain PID and the RCAC PID controller as the total inlet temperature  $T_0$  is varied. The figures in the top row show the thrust generated by the SFRJ, the performance variable on a logarithmic scale is shown in the middle row, and the figures in the bottom row show the control signal. Note that RCAC adjusts the controller gains continually to improve the transient response.

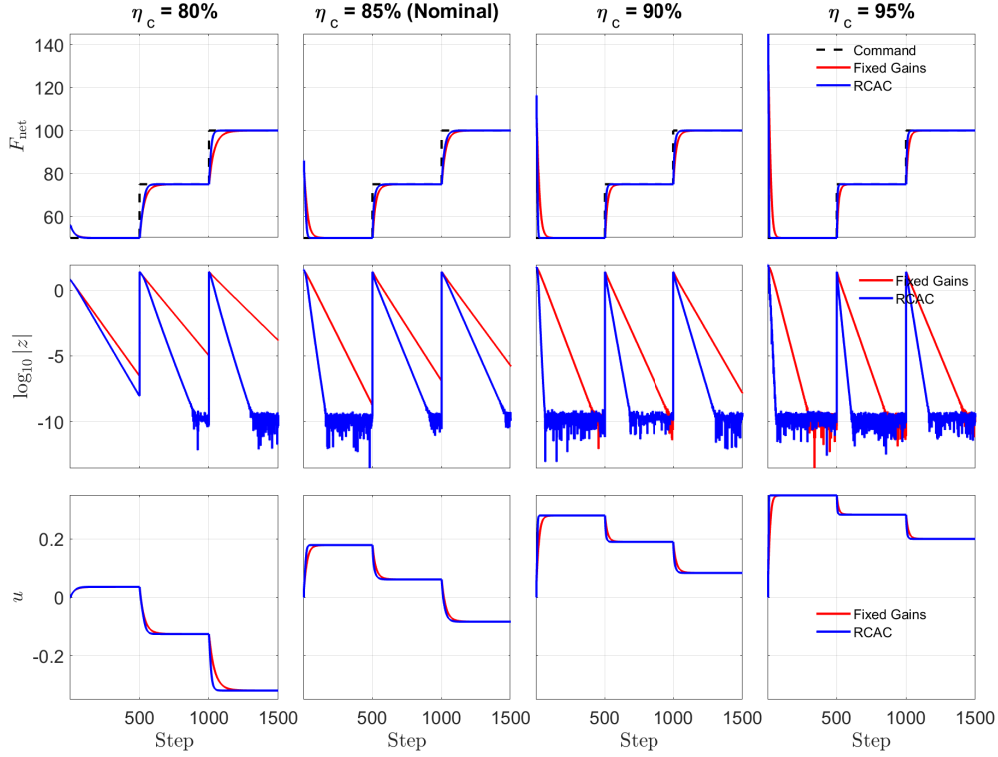


Fig. 9 Closed-loop response of the SFRJ with the fixed-gain PID and the RCAC PID controller as the combustion efficiency  $\eta_c$  is varied. The figures in the top row show the thrust generated by the SFRJ, the performance variable on a logarithmic scale is shown in the middle row, and the figures in the bottom row show the control signal. Note that RCAC adjusts the controller gains continually to improve the transient response.

## V. Conclusion

In this paper, we developed an adaptive PID controller, based on retrospective cost adaptive control algorithm, to regulate the thrust generated by a simplified model of a solid fuel ramjet, without using any modeling information. As a first step towards developing a learning-based controller to regulate the thrust generated by an SFRJ, we developed a static model of an SFRJ based on steady-state thermodynamic relations. The adaptive PID controller was then integrated with the SFRJ simulation and tuned to obtain an acceptable transient performance. The adaptive PID controller is shown to be robust to operating conditions and uncertainties in the SFRJ model. In fact, in all scenarios simulating uncertain conditions, the adaptive PID controller outperforms the fixed-gain PID controller. In our future work, we will replace the static SFRJ model with a dynamic SFRJ model and demonstrate thrust regulation with a learning controller.

## VI. Acknowledgment

This work was supported in part by the 2022 Naval Innovative Science and Engineering (NISE) program.

## References

- [1] Netzer, D. W., "Modeling solid-fuel ramjet combustion," *Journal of Spacecraft and Rockets*, Vol. 14, No. 12, 1977, pp. 762–766.
- [2] Stevenson, C. A., and Netzer, D. W., "Primitive-variable model applications to solid-fuel ramjet combustion," *Journal of Spacecraft and Rockets*, Vol. 18, No. 1, 1981, pp. 89–94.
- [3] Ben-Arosh, R., Natan, B., Spiegler, E., and Gany, A., "Theoretical study of a solid fuel scramjet combustor," *Acta Astronautica*, Vol. 45, No. 3, 1999, pp. 155–166.
- [4] Sun, B., Wu, X.-s., Cai, W.-x., and Xia, Q., "Numerical Simulation of Pitot Solid Fuel Ramjets," *2009 International Conference on Computational Intelligence and Software Engineering*, 2009, pp. 1–4. <https://doi.org/10.1109/CISE.2009.5365984>.
- [5] Wang, L., Wu, Z., Chi, H., Liu, C., Tao, H., and Wang, Q., "Numerical and experimental study on the solid-fuel scramjet combustor," *Journal of Propulsion and Power*, Vol. 31, No. 2, 2015, pp. 685–693.
- [6] Campbell Jr, W., Ko, B., Lowe, S., and Netzer, D., "Solid-fuel ramjet fuel regression rate/thrust modulation," *Journal of Propulsion and Power*, Vol. 8, No. 3, 1992, pp. 624–629.
- [7] Pelosi-Pinhas, D., and Gany, A., "Bypass-regulated solid fuel ramjet combustor in variable flight conditions," *Journal of propulsion and power*, Vol. 19, No. 1, 2003, pp. 73–80.
- [8] Pei, X., Wu, Z., Wei, Z., and Liu, J., "Numerical investigation on internal regressing shapes of solid-fuel scramjet combustor," *Journal of Propulsion and Power*, Vol. 29, No. 5, 2013, pp. 1041–1051.
- [9] MacLeod, C., and Gerrard, C. E., "A review of air-fuel mixing and alternative methods in scramjets and scramjet-like engines," *Journal of the British Interplanetary Society*, Vol. 69, No. 4, 2016.
- [10] Jarymowycz, T., Yang, V., and Kuo, K., "Numerical study of solid-fuel combustion under supersonic crossflows," *Journal of Propulsion and Power*, Vol. 8, No. 2, 1992, pp. 346–353.
- [11] Durali, M., Alemohammad, S., and Alasty, A., "Propulsion control of a solid fuel ramjet using a robust adaptive neural controller," *Proceedings of 2005 IEEE Conference on Control Applications, 2005. CCA 2005.*, 2005, pp. 879–884. <https://doi.org/10.1109/CCA.2005.1507240>.
- [12] Durali, M., and Alemohammad, H., "Velocity Regulation of a Solid Fuel Ramjet Using Neural Networks and Adaptive Sliding Control," *ASME International Mechanical Engineering Congress and Exposition*, Vol. 42169, 2005, pp. 239–248.
- [13] Goel, A., Xie, A., Duraisamy, K., and Bernstein, D. S., "Retrospective cost adaptive thrust control of a 1D scramjet with Mach number disturbance," *2015 American Control Conference (ACC)*, 2015, pp. 5551–5556. <https://doi.org/10.1109/ACC.2015.7172208>.
- [14] Goel, A., Duraisamy, K., and Bernstein, D. S., "Retrospective cost adaptive control of unstart in a model scramjet combustor," *AIAA Journal*, Vol. 56, No. 3, 2018, pp. 1085–1096.
- [15] Goel, A., Duraisamy, K., and Bernstein, D., "Output-Constrained Adaptive Control for Unstart Prevention in a 2D Scramjet Combustor," *AIAA Scitech 2019 Forum*, 2019, p. 0927.

- [16] Evans, J. V., Senior, W. C., Gejji, R. M., and Slabaugh, C. D., “Performance of a Solid-Fuel Ramjet Combustor with Bypass Air Addition,” *Journal of Propulsion and Power*, 2022, pp. 1–9.
- [17] Gordon, S., and McBride, B. J., “Computer Program for Calculation of Complex Chemical Equilibrium Compositions and Applications,” *NASA Reference Publication 1311*, 1996.
- [18] Zucrow, M. J., and Hoffman, J. D., *Gas dynamics. volume 1*, Wiley, 1976.
- [19] Rahman, Y., Xie, A., and Bernstein, D. S., “Retrospective Cost Adaptive Control: Pole Placement, Frequency Response, and Connections with LQG Control,” *IEEE Control System Magazine*, Vol. 37, 2017, pp. 28–69. <https://doi.org/10.1109/MCS.2017.2718825>.
- [20] Kamaldar, M., Islam, S. A. U., Sanjeevini, S., Goel, A., Hoagg, J. B., and Bernstein, D. S., “Adaptive digital PID control of first-order-lag-plus-dead-time dynamics with sensor, actuator, and feedback nonlinearities,” *Advanced Control for Applications*, Vol. 1, No. 1, 2019, p. e20. <https://doi.org/10.1002/adc2.20>.
- [21] Goel, A., U. Islam, S. A., and Bernstein, D. S., “Adaptive Control of MIMO Systems Using Sparsely Parameterized Controllers,” *2020 American Control Conference (ACC)*, 2020, pp. 5340–5345. <https://doi.org/10.23919/ACC45564.2020.9147513>.
- [22] Islam, S. A. U., and Bernstein, D. S., “Recursive Least Squares for Real-Time Implementation,” *IEEE Control Systems Magazine*, Vol. 39, No. 3, 2019, pp. 82–85. <https://doi.org/10.1109/MCS.2019.2900788>.